Variability and Trends in Surface Meteorology and Air–Sea Fluxes at a Site off Northern Chile

ROBERT A. WELLER

Woods Hole Oceanographic Institution, Woods Hole, Massachusetts

(Manuscript received 22 August 2014, in final form 16 December 2014)

ABSTRACT

Time series of surface meteorology and air–sea exchanges of heat, freshwater, and momentum collected from a long-term surface mooring located 1600 km west of the coast of northern Chile are analyzed. The observations, spanning 2000–10, have been withheld from assimilation into numerical weather prediction models. As such, they provide a unique in situ record of atmosphere–ocean coupling in a trade wind region characterized by persistent stratocumulus clouds. The annual cycle is described, as is the interannual variability. Annual variability in the air–sea heat flux is dominated by the annual cycle in net shortwave radiation. In austral summer, the ocean is heated; the 9-yr mean annual heating of the ocean is 38 W m^{-2}. Ocean cooling is seen in 2006–08, coincident with La Niña events. Over the full record, significant trends were found. Increases in wind speed, wind stress, and latent heat flux over 9 yr were 0.8 m s^{-1}, 0.022 N m^{-2}, and 20 W m^{-2} or 13%, 29%, and 20% of the respective 9-yr means. The decrease in the annual mean net heat flux was 39 W m^{-2} or 104% of the mean. These changes were found to be largely associated with spring and fall. If this change persists, the annual mean net air–sea heat flux will change sign by 2016, when the magnitude of the wind stress will have increased by close to 60%.

1. Introduction

The focus here is on the surface meteorology and air–sea fluxes of heat, freshwater, and momentum at an oceanic site at 20°S, 85°W in the South Pacific Ocean, some 1600 km west of the coast of northern Chile. This is a region characterized by southeast trade winds, a dominance of evaporation over precipitation, a strong annual cycle in insolation associated with its proximity to the Tropic of Capricorn, and the infrequent occurrence of propagating synoptic weather systems because of the proximity of the Andes. At the same time it is a data-sparse region marked by the presence of low marine stratus clouds, and, like other eastern boundary regions of ocean basins, it is a region that has presented challenges to climate modelers (Large and Danabasoglu 2006; Zheng et al. 2011).

A recent international collaborative research effort called the Variability of the American Monsoon Systems (VAMOS) Ocean–Cloud–Atmosphere–Land Study (VOCALS) was conducted there in 2008 (Mechoso et al. 2013). The goals of VOCALS were to better quantify ocean–atmosphere coupling, to improve understanding of the processes that govern the sea surface temperature (SST) and the amount and type of clouds, and thus to make progress on reducing the systematic regional errors in coupled ocean–atmosphere general circulation models (Mechoso et al. 2013). Beyond the desire to better understand the atmospheric and oceanic processes at work in the region, work there is motivated by the belief that this region influences a broader Pacific area (Ma et al. 1996; Manganello and Huang 2009). Further, the trade winds there drive a large area of upwelling along the coast that has high biological productivity. Because of the societal value of this coastal ecosystem, there is also interest in examining the impacts of variability and change in the trade winds on the productivity of the upwelling regime (Demarcq 2009; Narayan et al. 2010).

In addition, the eastern South Pacific draws interest because SST there is cooling while in most regions it is warming. Recently, Kosaka (2014) looked at surface winds and sea surface temperatures across the Pacific

Denotes Open Access content.

Corresponding author address: Robert A. Weller, Woods Hole Oceanographic Institution, 266 Woods Hole Road, Woods Hole, MA 02543.
E-mail: rweller@whoi.edu

DOI: 10.1175/JCLI-D-14-00591.1

and postulated that increasing trade winds in the Pacific as seen in reanalysis fields were responsible for cooling in the eastern Pacific that has led to a decrease in the rate of global warming of sea surface temperatures. Similarly, England et al. (2014) report finding increasing trade winds in the equatorial and eastern Pacific over the years from 1992 to 2011 in the same Interim European Centre for Medium-Range Weather Forecasts (ECMWF) Re-Analysis (ERA-Interim) and link cooling in the eastern Pacific to those stronger winds.

Our effort to investigate the surface meteorology and air–sea fluxes in this region has been made possible by the maintenance of a long-term surface mooring located close to 20°S, 85°W. Over the last 10–15 yr, ocean observing technology has advanced, and surface moorings are now capable of being used as platforms to collect accurate, long running time series of surface meteorology; air–sea exchanges of heat, momentum, and freshwater and oceanic temperature; salinity; and velocity. A small number of these surface moorings have been established as ocean reference stations (ORS), where care is dedicated to collecting observations with state of the art accuracies and where the data are withheld from assimilation into numerical model fields and from inclusion in fields derived from combinations of model and remote sensing data. In this paper, we examine the first 10 yr of data collected from the ORS established in the eastern South Pacific at 20°S, 85°W, some 1600 km west of northern Chile, in this region characterized by persistent marine stratus clouds.

The first 10 yr of observations support an improved characterization of the region offshore off northern Chile in the southeastern Pacific. There are found to be persistent trade winds and weak mean heating of the ocean by the atmosphere combined with a dominance of evaporation over precipitation. There is an annual cycle in the heat exchange and in sea surface and air temperature. There is also evidence of the interannual variability, possibly associated with ENSO. There are significant trends observed in both the wind speed and in the net air–sea heat flux, with winds increasing from an annual mean of 5.7 m s^{-1} in 2001 to an annual mean of 6.5 m s^{-1} in 2009 and the annual mean net heat flux decreasing from 60.4 W m^{-2} in 2001 to 21.2 W m^{-2} in 2009, with a positive value of heat flux indicating heating of the ocean by the atmosphere.

Other studies have addressed the synoptic meteorology and diurnal variability in the lower atmosphere in the region (Rahn and Garreaud 2010a,b; Toniazzo et al. 2011). We focus here on utilizing the 10-yr record of the surface meteorology and air–sea flux records at the ORS Stratus Deck Regions of the Eastern Pacific (STRATUS) to quantify the annual, interannual, and longer-term variability. In part, this is done so that this analysis of the accurate and withheld surface buoy data will be available for comparison to variability and trends seen in other representations of the surface meteorology and air–sea fluxes in the eastern South Pacific off northern Chile. After summarizing the observational methods, an overview of the surface meteorology and air–sea fluxes is provided, and then the mean annual signals, the departures from the mean annual record on interannual time scales, and the trends over the first 10 yr are discussed. A discussion of the findings in the context of other work follows. An effort is made here to identify and quantify the robust signals found on annual, interannual, and longer time scales in the withheld data from the ORS STRATUS so that others can investigate if they are accurately replicated in models. The URL where the data can be obtained is included in the conclusions section.

2. Observational methods

Close to 20°S, 85°W, some 1600 km west of northern Chile, a surface mooring has been in place since October 2000 in water depths of close to 4500 m. The mooring and the instrumentation are described in Colbo and Weller (2007). The meteorological instrumentation on the surface buoy provide the data discussed here, and the accuracies of the meteorological data and of the air–sea fluxes of heat, freshwater, and momentum derived from them are discussed by Colbo and Weller (2009). In brief, two independent improved meteorology (IMET) instrument packages (Hosom et al. 1995) mounted on the buoy support two sets of redundant sensors measuring wind speed and direction, air temperature and humidity, sea surface temperature and salinity, incoming shortwave radiation, incoming longwave radiation, barometric pressure, and rain rate. For some key parameters, such as wind speed and relative humidity, a third set of sensors is added. Meteorological sensors are mounted close to 3 m above the sea surface, and several temperature sensors are mounted on the buoy hull just below the waterline and on the bridle below the buoy hull. The raw measurements for each parameter are averaged, and the averages are recorded once per minute. The surface buoy records the 1-min data internally as well as transmitting hourly averaged data for the duration of its deployment, typically 1 yr. Every year a fresh mooring and surface buoy are deployed on the cruise that also recovers the buoy and mooring that have been in service. The exact locations of the sites where the moorings have been anchored each year are given in the appendix; they have been selected to meet the requirement for an area of flat bottom topography as a target when dropping the anchor combined with the desire to alternate sites to reduce the amount of fishing gear that accumulates on the mooring line and moored

TABLE 1. Accuracies of buoy meteorological sensors based on laboratory and field calibrations and intercomparisons and given for monthly and longer time scales.

Sensor	Accuracy
Incoming shortwave	4 W m^{-2}
Incoming longwave	5 W m^{-2}
Relative humidity (RH)	1%–2%
Air temperature	0.1°C
Barometric pressure	0.2 hPa
Sea surface temperature	0.04°C
Wind speed	1%; at least 0.1 m s^{-1}
Wind direction	5°
Precipitation	20%

TABLE 2. Accuracies of the computed fluxes at monthly time scales.

Flux	Accuracy
Net longwave	2 W m^{-2}
Net shortwave	3 W m^{-2}
Latent	4 W m^{-2}
Sensible	1.5 W m^{-2}
Net heat flux	8 W m^{-2}
Wind stress	0.007 N m^{-2}
Freshwater flux	20%

instrumentation. Two general locations, just to the southwest and to the northwest of 20°S, 85°W, have been used with a maximum distance between mooring sites of 80 km.

From October 2000 to July 2010, when the mooring line of the buoy then present failed, allowing the surface buoy to drift off the station, continuous observations are available; it is this nearly 10-yr-long time series that is discussed here. Satellite wind and blended surface meteorological products and shipboard observations taken from the mooring cruises over the years (De Szoeke et al. 2010) have shown general homogeneity in the region within 100 km of 20°S, 85°W when looking at the surface meteorology and air–sea fluxes on time scales longer than daily, so we have here merged the data from the 10 deployments into one time series taken to be characteristic of the region near 20°S, 85°W. Occupation of the site was resumed in April 2011 and continues to date.

The challenges of developing robust and accurate, unattended meteorological quantifying the performance of the sensors when deployed unattended on a buoy for 1 yr have been addressed in our work over several decades. New, more robust meteorological packages for use on ships and buoys have been developed (Hosom et al. 1995) and are in commercial production. Very stable signal-conditioning electronics have been developed, and sensors are equipped with appropriate housings (e.g., passive radiation shields to minimize solar heating of air temperature and humidity sensors, porous Teflon filters for humidity sensors, and pressure ports that reduce the impact of dynamic pressure fluctuations on the barometric pressure sensor). Collaborative field efforts, such as the Tropical Ocean Global Atmosphere (TOGA) Coupled Ocean–Atmosphere Response Experiment (COARE), that focused on obtaining and verifying accurate measurements of the air–sea fluxes of heat, freshwater, and momentum have left a legacy of best practices (Weller et al. 2004) and improved formulas for computing the air–sea fluxes from mean meteorological observables (Fairall et al. 1996). Among the lessons learned have been the need for and value of the deployment of redundant sensors on each platform and the critical role of sensor intercomparisons conducted in the field in conjunction with careful laboratory.

Preparation of the surface buoy for each deployment includes laboratory calibration before and after the deployment and running the buoy on land as it will be deployed and examining sensor performance for problems (e.g., radio frequency or magnetic interference) both at home and after shipment to the port where the gear is loaded. At sea, over the years we have adopted the practice of deploying the new mooring before recovering the old mooring in order to collect several days of overlapping data. During this intercomparison period, data from an independent set of well-calibrated sensors on the research vessel are also collected with the ship stationed bow into the wind, close to and downwind of each buoy. The overlapping time series of the two buoys and the additional record from the ship are key to identifying any drift or degradation in the sensors after 1 yr at sea as well as to identifying more significant failure modes. On occasion, some sensors have been damaged upon recovery, preventing the postdeployment calibration, further elevating the importance of these in situ comparisons.

Based on the approaches summarized above, the accuracies of the meteorological sensors obtained on the buoys are shown in Table 1. Shortwave and longwave accuracies are limited by the motion of the buoy as well by the sensors. In persistent low winds and strong insolation, air temperature and humidity sensors are impacted by solar heating. Compass performance and flow distortion impact wind velocity accuracies. Errors stemming from pitch and roll of the buoy, solar heating, and other transient conditions are reduced in averages such as monthly. Further discussions of the instrumentation and sensors are given by Colbo and Weller (2009), Weller et al. (2012), and Bigorre et al. (2013).

The meteorological data are used together with empirical formulas to calculate the net longwave radiation, the net shortwave radiation, the latent and sensible heat

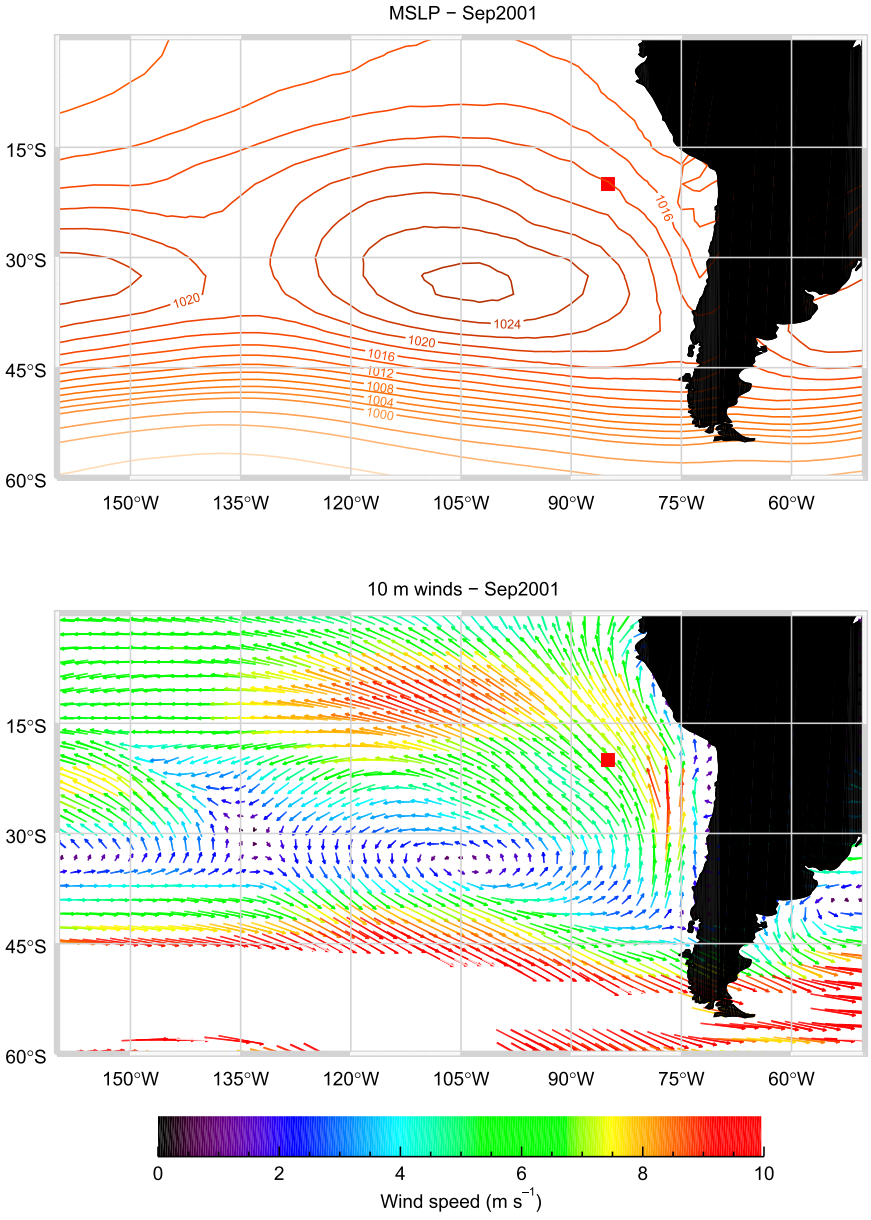

FIG. 1. (top) Mean sea level pressure (hPa) for September 2001 from the NCEP–DOE Reanalysis-2. (bottom) Mean 10-m wind vectors ($m\,s^{-1}$) for September 2001 from the NCEP–DOE Reanalysis-2. For both, the red square marks the location of the long-term ORS STRATUS.

fluxes, the wind stress, and the freshwater flux. The computation of the fluxes is done using hourly meteorological data. A near-surface current meter provides a proxy for surface current, and wind speed and wind velocity relative to the surface current are used in the computations. The net heat flux is the sum of the net shortwave radiation, the net longwave radiation, the sensible heat flux, and the latent heat flux, with a positive sign used to indicate heat flowing into the ocean. The formulas and the propagation of sensor uncertainty through the computations are discussed in Colbo and Weller (2009); for sensible and latent heat fluxes and for wind stress, version 3.0 of the COARE flux algorithm (Fairall et al. 1996) was used. Table 2 summarizes the accuracies associated with the flux time series discussed here. These hold for wind conditions below $20\,m\,s^{-1}$, as experienced at the mooring site. Errors in heat flux components are of opposite sign and cancel, leading to a total error in net heat flux smaller than the sum of the magnitudes of the errors in the components.

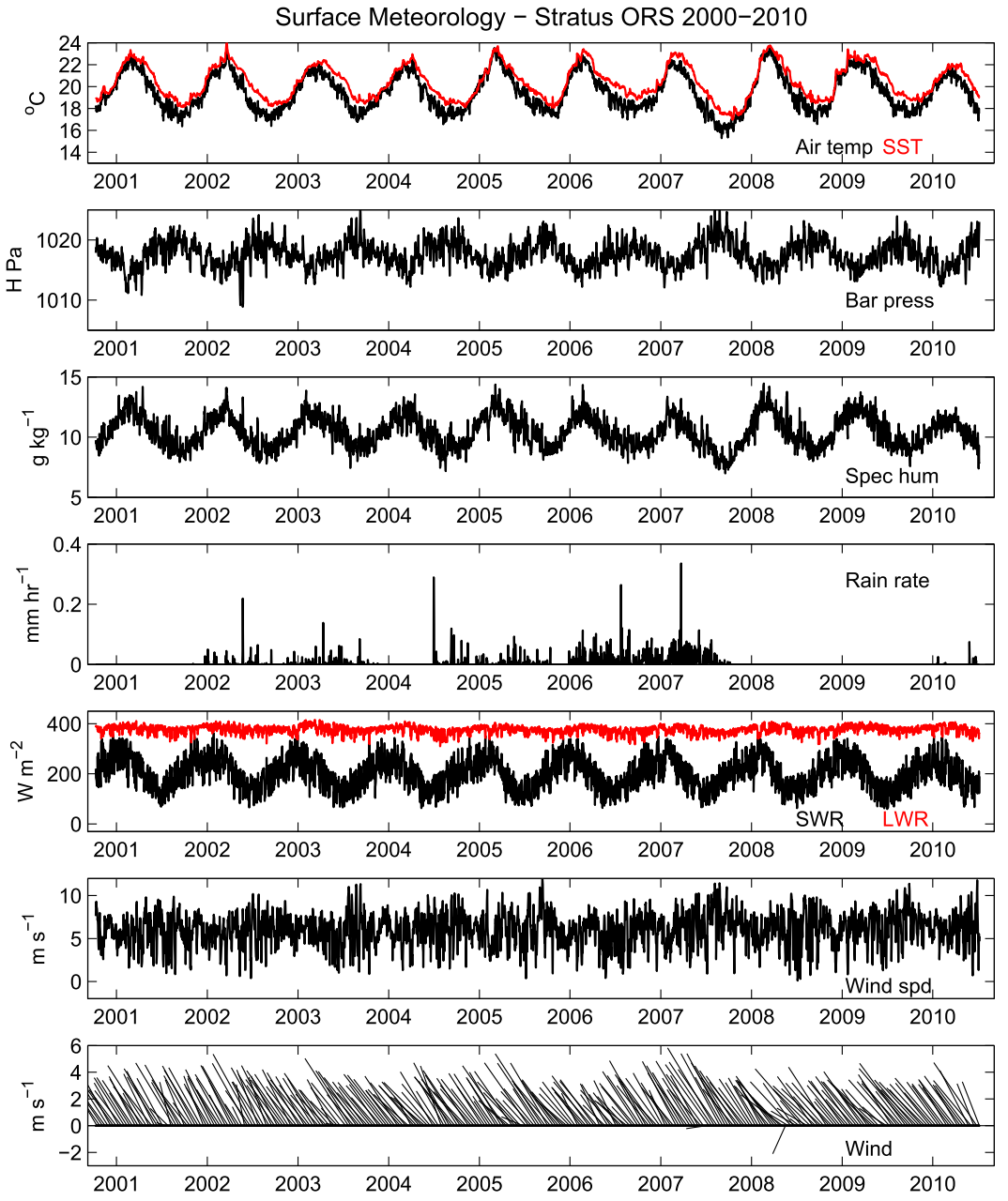

FIG. 2. Surface meteorological time series from the ORS STRATUS. All time series are of daily averages: (top)–(bottom) air temperature (black) and sea surface temperature (red); barometric pressure; rain rate; incoming shortwave (black) and longwave (red) radiation; wind speed; and the low-passed (running mean over ±5 days) wind vectors plotted once per 10 days.

3. Overview of the ORS STRATUS record from 2000 to 2010

The mooring is located to the north and east of the typical location of the South Pacific anticyclone in an area of well-developed southeast trade winds (Fig. 1). Time series of daily averages of the surface meteorological properties from 2000 to 2010 are shown in Fig. 2 as measured at the heights of the sensors above the sea surface, 2.4 m for the pressure sensor, 2.3 m for the humidity and air temperature sensors, 2.7 m for the anemometer, 2.8 m for the radiometers, and a depth of 1.0 m for sea surface temperature and salinity. Wind velocity is a vector that points in the direction the wind is flowing toward. Figure 3 shows the 2000–10 time series of the daily averaged net heat flux, the four components of the

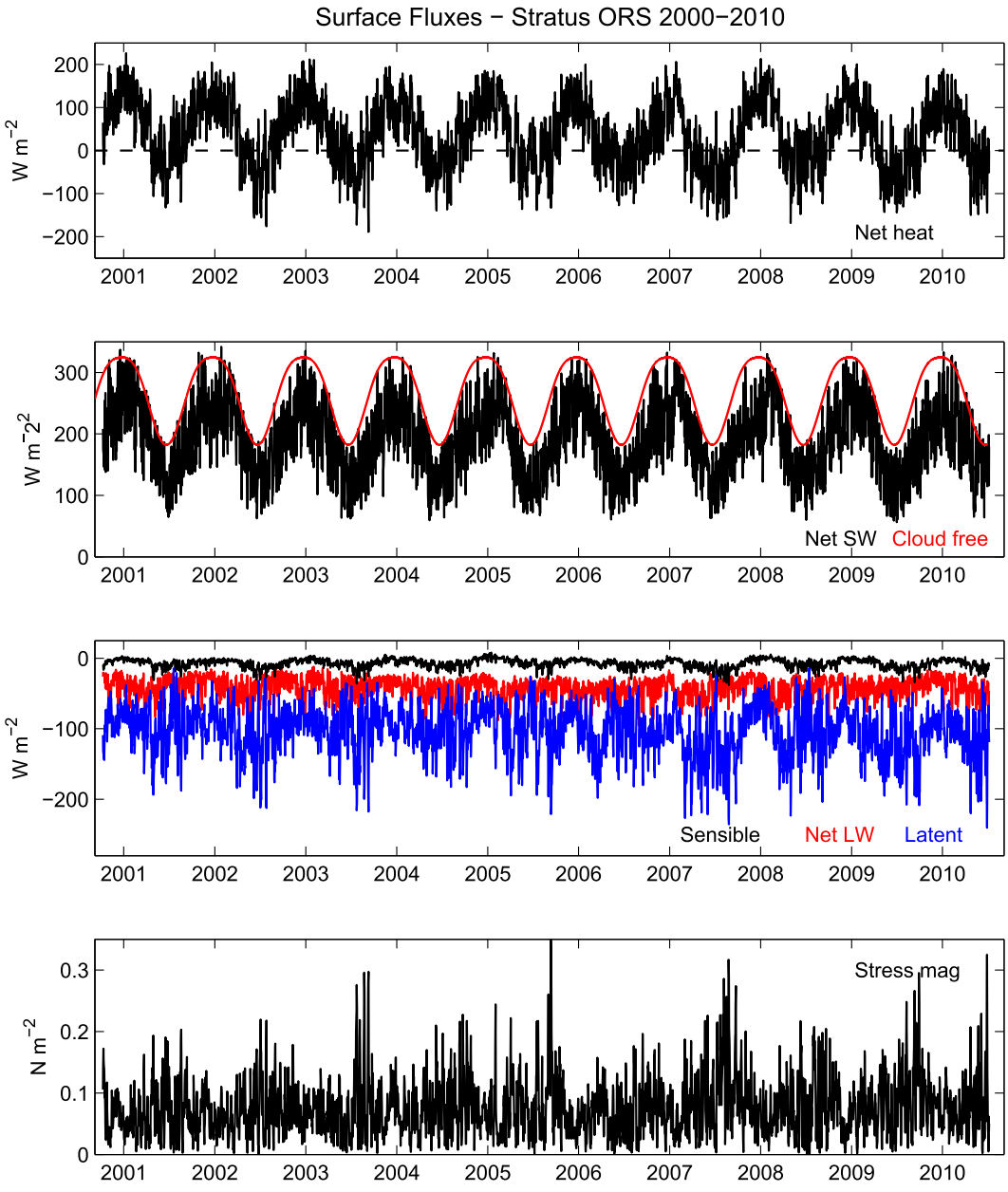

FIG. 3. Time series of daily averages of the surface fluxes from the ORS STRATUS from 2000 to 2010: (top)–(bottom) the net heat flux; the net shortwave radiation (black) with a low-pass-filtered (48 h) theoretical, clear-sky net shortwave radiation in red; the sensible heat flux (black), net longwave radiation (red), and latent heat flux (blue); and the magnitude of the wind stress.

neat heat flux: net shortwave radiation, net longwave radiation, latent heat flux, and sensible heat flux), and the magnitude of the wind stress. Long-term means were computed from 1 January 2001 to 31 December 2009 (inclusive). The surface meteorological means are given in Table 3, and the flux means are given in Table 4.

The trade winds vary in speed, as seen in Fig. 2, but were dominant from the southeast. In wind rose plots, 45% of the daily vectors fell in one 5°-wide bin and 95% fell within ±7.5° of the mean direction. The steadiness of the wind velocity, the ratio of the mean vector wind speed to the mean scalar wind speed, was 0.94, computed from hourly data. The spectrum of the wind velocity was red (having more energy at lower frequencies) at periods shorter than about 8 days and had a plateau spanning periods between 8 days and 1 yr; there was not a significant peak in the wind spectrum at the period of 1 yr. Spectra were computed using the hourly time

TABLE 3. Annual means for basic observables from the surface mooring of the ORS STRATUS for the first 9 yr together with the 9-yr means. Shown, as observed at the height of the sensors are air temperature (air T); ocean temperature (sea T); relative humidity (RH); specific humidity (SH); barometric pressure (BP); salinity (sal) and density anomaly (sigma) at −1.0 m; incoming shortwave and longwave radiation (SWin and LWin, respectively) at 2.8 m; and wind speed ($|\mathbf{U}|$), wind direction (dir), and east and north (positive toward) wind components (U and V, respectively) at 2.7 m.

	2001	2002	2003	2004	2005	2006	2007	2008	2009	Mean
Air T (°C)	19.50	19.39	19.48	19.31	19.81	19.55	18.80	19.93	19.75	19.53
Sea T (°C)	20.39	20.37	20.42	20.10	20.50	20.63	19.84	20.70	20.73	20.41
RH (%)	74.9	73.6	74.6	74.5	74.6	72.8	73.0	73.8	73.7	74.02
SH ($g\,kg^{-1}$)	10.6	10.3	10.6	10.4	10.7	10.3	9.8	10.7	10.5	10.4
BP (hPa)	1017.5	1017.6	1017.8	1017.8	1017.7	1017.2	1018.2	1017.6	1017.3	1017.6
SWin ($W\,m^{-2}$)	215.0	209.9	197.4	198.3	204.6	200.2	202.3	207.2	194.7	202.1
LWin ($W\,m^{-2}$)	378.3	376.7	379.8	373.9	374.3	373.5	372.2	375.7	382.0	376.3
$\|\mathbf{U}\|$ ($m\,s^{-1}$)	5.71	5.94	6.02	6.13	6.09	5.76	6.56	6.18	6.47	6.07
U ($m\,s^{-1}$)	−4.26	−4.33	−5.00	−5.08	−5.04	−4.71	−5.25	−4.94	−5.59	−4.92
V ($m\,s^{-1}$)	3.33	3.52	3.06	3.10	3.06	2.93	3.72	3.26	2.96	3.14
Dir (°)	298	301	300	297	298	294	303	298	295	303
Sal (psu)	35.44	35.44	35.49	35.41	35.45	35.33	35.29	35.39	35.47	35.41
Sigma ($g\,kg^{-1}$)	24.99	24.99	25.01	25.04	24.97	24.85	25.02	24.86	24.92	24.96

series, with band averaging increasing with frequency. The 95% confidence estimates were computed based on the degrees of freedom in the averaging for each spectral estimate. Peaks were judged to be significant when they were larger than the envelope given by the confidence limits. In contrast to the wind, air temperature, SST, barometric pressure, specific humidity, and incoming shortwave radiation had evident annual cycles (Fig. 2). Spectra of the hourly air and sea surface temperatures and of hourly incoming longwave radiation were red, with significant peaks at periods of close to 1 yr, 24 h, and 12 h. Hourly incoming shortwave radiation had sharp spectral peaks at 24 h, 12 h, and shorter harmonics because of the periodic but nonsinusoidal shape of the daily signal; there was also a peak at the 1-yr period.

On average over these nine years, the ocean gained $37.6\,W\,m^{-2}$ from the atmosphere, with the annual shortwave gain more than compensating for the losses associated with latent, sensible, and net longwave radiation. The latent heat flux was equivalent to an evaporation of $1.3\,m\,yr^{-1}$ over the nine years, and the rain rate was $0.04\,m\,yr^{-1}$, so the average freshwater loss was close to $1.3\,m\,yr^{-1}$. Net heat flux variability was dominated by the contribution from the net shortwave radiation and thus had a strong annual spectral peak. In Fig. 3, after Cronin et al. (2006) and Iqbal (1988), the 48-h low-pass filtered, predicted, cloud-free, incoming surface shortwave radiation is overplotted on the observed daily surface net shortwave radiation, and the greater difference between that and the observed incoming shortwave radiation indicates there were more clouds in austral spring and summer.

In a number of variables, there was evidence in Figs. 2 and 3 of interannual variability: for example, in the cooler air and sea surface temperatures in the latter part of 2007. There was also the appearance in some observables (e.g., wind speed) of an overall trend. To look further, as described in the sections to follow, we isolated the average annual cycle, removed the annual cycle to highlight interannual variability, and analyzed seasonal and annual means for evidence of statistically significant trends.

TABLE 4. Annual means for heat fluxes and wind stress for the nine full years of ORS STRATUS data, and the mean of the nine years. Rows show net heat flux (QN), latent heat flux (QH), sensible heat flux (QB), net shortwave radiation (SWnet), net longwave radiation (LWnet), the skin temperature calculated for use in computing the heat flux (SST), the magnitude of the wind stress ($|\boldsymbol{\tau}|$), the east component of the wind stress (τ_x), and the north component of the wind stress (τ_y).

	2001	2002	2003	2004	2005	2006	2007	2008	2009	Mean
QN ($W\,m^{-2}$)	60.4	43.6	41.3	39.3	44.2	25.3	22.0	38.8	21.2	37.6
QH ($W\,m^{-2}$)	−94.8	−104.7	−99.3	−98.5	−98.8	−108.9	−115.6	−105.8	−115.1	−103.5
QB ($W\,m^{-2}$)	−7.3	−8.1	−6.7	−6.4	−5.3	−8.7	−10.2	−6.4	−8.9	−7.3
SWnet ($W\,m^{-2}$)	203.1	198.4	186.5	187.4	193.4	189.2	191.2	195.8	184.0	191.0
LWnet ($W\,m^{-2}$)	−40.6	−41.9	−39.2	−43.2	−45.0	−46.4	−43.4	−44.8	−38.8	−42.6
SST (°C)	20.22	20.18	20.24	19.93	20.32	20.43	19.65	20.52	20.55	20.23
$\|\boldsymbol{\tau}\|$ ($N\,m^{-2}$)	0.0655	0.0712	0.0746	0.0759	0.0769	0.0694	0.0915	0.0795	0.0874	0.0754
τ_x ($N\,m^{-2}$)	−0.0500	−0.0527	−0.0624	−0.0634	−0.0637	−0.0573	−0.0735	−0.0644	−0.0762	−0.0616
τ_y ($N\,m^{-2}$)	0.0388	0.0420	0.0384	0.0383	0.0399	0.0358	0.0525	0.0429	0.0401	0.0397

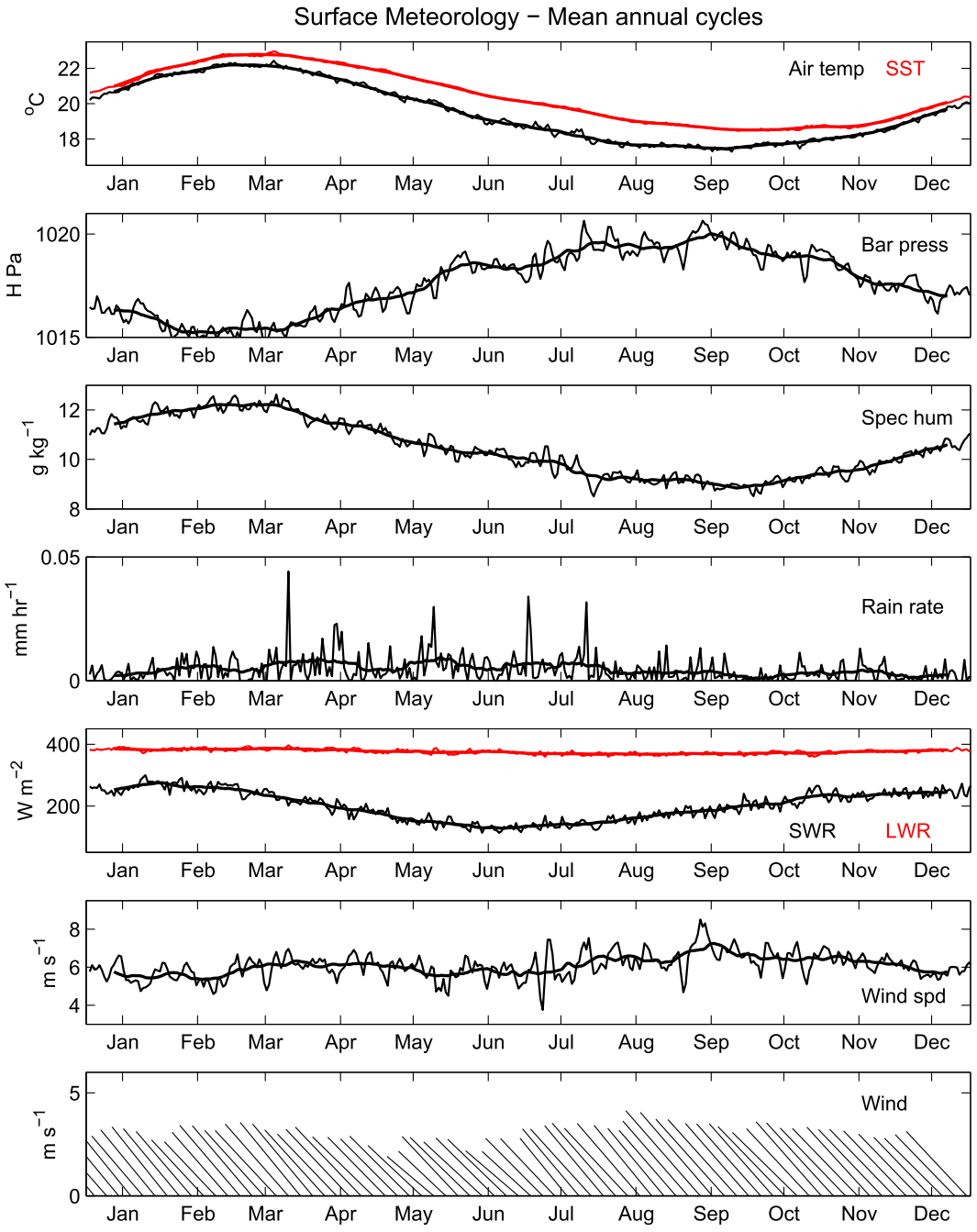

FIG. 4. Mean annual cycles of the surface meteorological variables at the ORS STRATUS, based on averaging nine calendar years, 2001–09. Daily values are the thin lines; thick lines are a 20-day running mean of the daily values. Shown are (top)–(bottom) air (black) and sea surface temperature (red); barometric pressure; specific humidity; rain rate; incoming shortwave (black) and longwave (red) radiation; wind speed; and the low-passed wind as vector sticks every 5 days.

4. The annual cycle

The nine full calendar years 2001–09 were used to determine the mean annual cycles, averaging the daily averages for the same day of each year. Figure 4 shows both the daily and 20-day low-passed time series of the annual cycles in surface meteorology, while Fig. 5 shows the annual cycles in the surface fluxes. Both air temperature and SST had sinusoidal signals of 5.2° and 4.5°C amplitude, respectively, where SST was always warmer

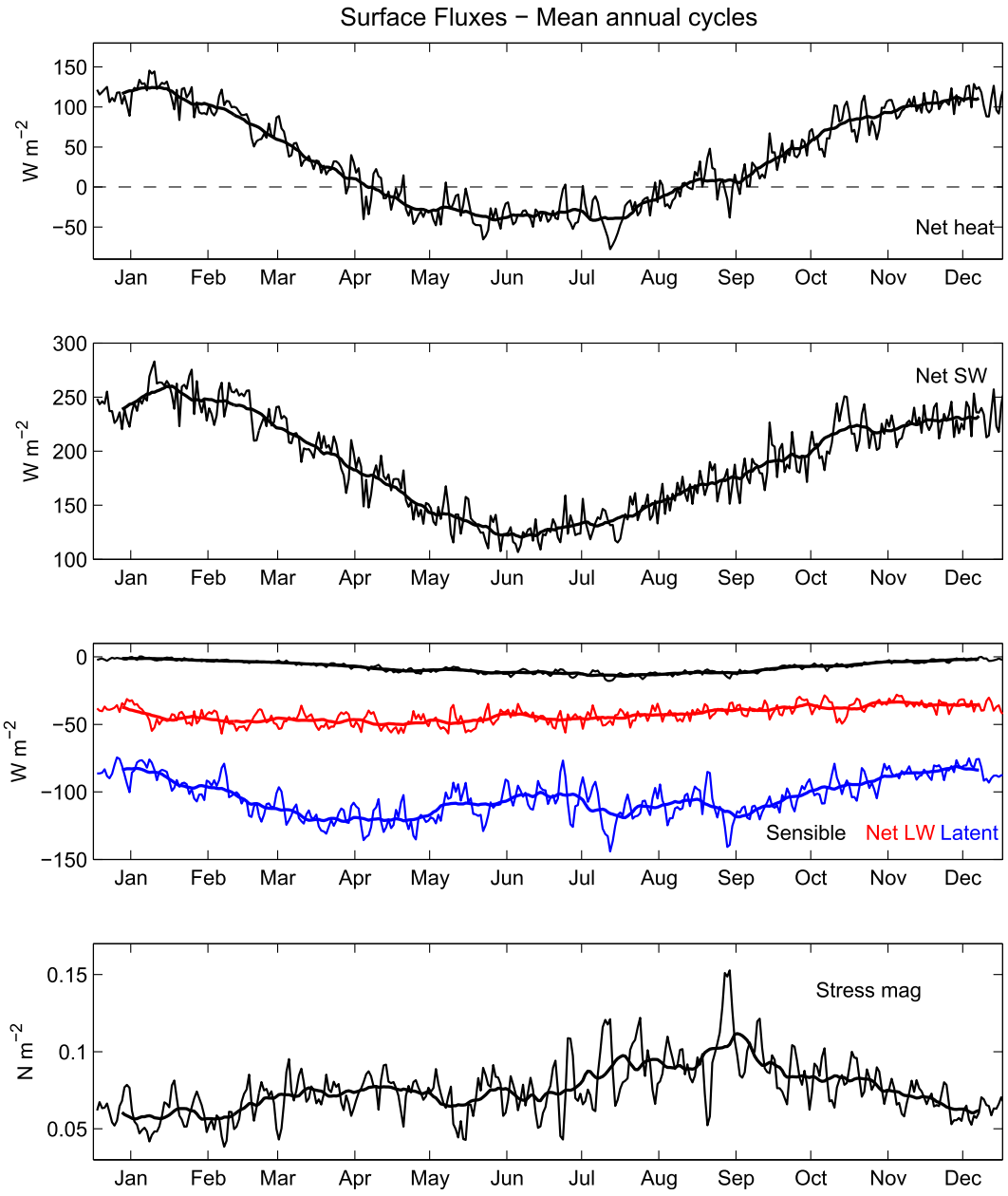

FIG. 5. The mean annual cycles of the air–sea heat fluxes and wind stress computed by averaging daily values from nine calendar years, 2001–09. The thin lines are daily values; the thick lines are a 20-day running mean. Shown are (top)–(bottom) net heat flux; net shortwave radiation; the sensible heat flux (black), net longwave heat flux (red), and latent heat flux (blue); and the magnitude of the wind stress.

than the air temperature. The warmest daily SST (air temperature) occurred on 19 March (19 March), and the coolest daily SST (air temperature) occurred on 26 September (23 September). The low-passed SST lagged the low-passed air temperature by 3–12 days. Specific humidity tracked air temperature, with lower values in association with cooler temperatures. Daily mean surface pressure was highest (1020.7 hPa) in mid-September and lowest (1014.6 hPa) in mid-March. Low-passed wind speed increased by $1.9\,\mathrm{m\,s^{-1}}$ with a maximum of $7.3\,\mathrm{m\,s^{-1}}$ coincident with the high in barometric pressure over the same time period. A seasonal cycle in incoming shortwave radiation was seen with a midwinter minimum of $127.6\,\mathrm{W\,m^{-2}}$ in low-passed incoming shortwave radiation and a summer maximum of $275.4\,\mathrm{W\,m^{-2}}$ with very little ($\sim 20\,\mathrm{W\,m^{-2}}$) variability in low-passed incoming longwave radiation over the year. Precipitation at the site was very light

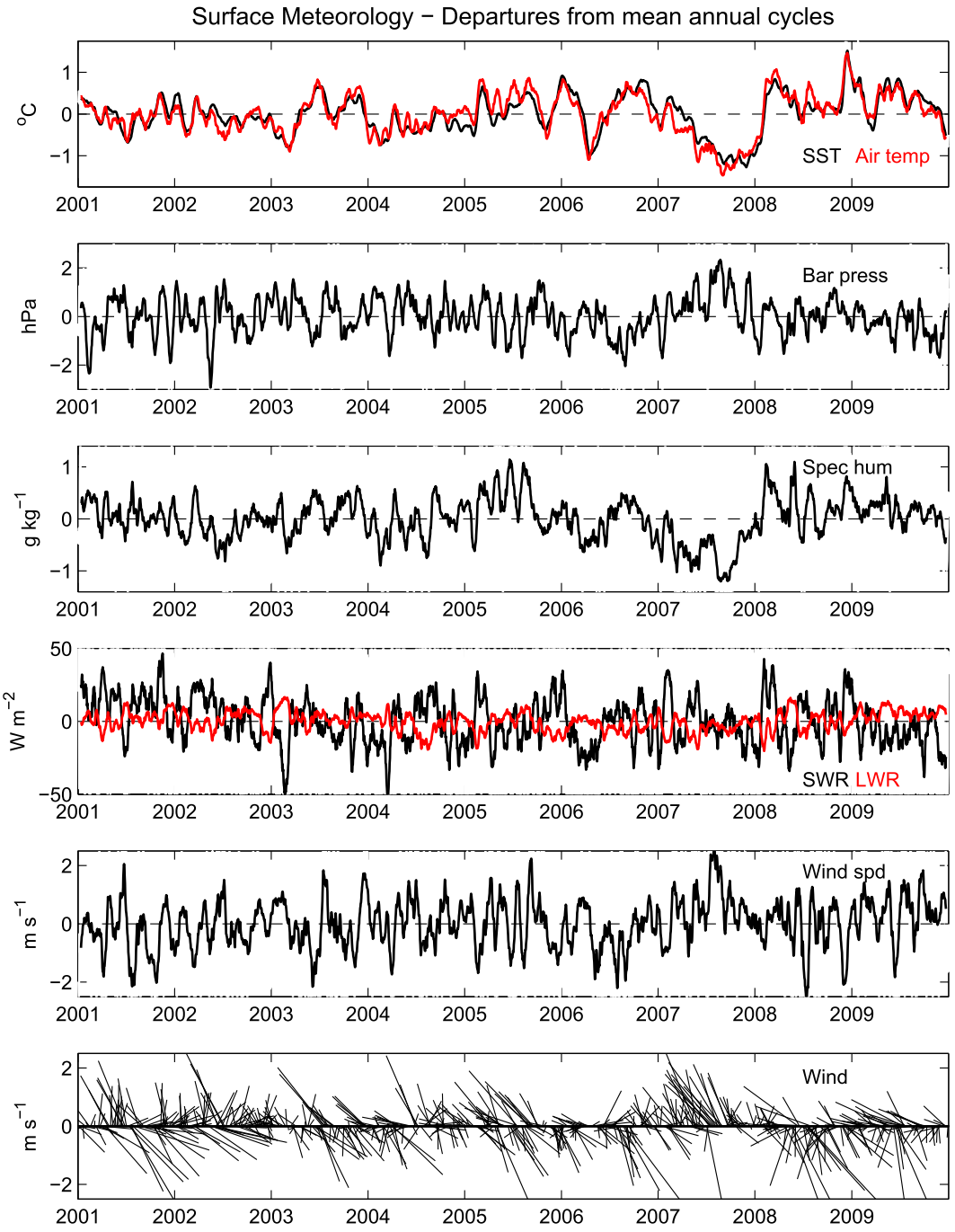

FIG. 6. Time series of the departures in daily averages of surface meteorology from the mean annual cycles, as shown in Fig. 4. All time series have had a 20-day running mean applied to the daily time series. Shown are (top)–(bottom) sea surface (black) and air temperature (red); barometric pressure; specific humidity; incoming longwave (red) and shortwave (black) radiation; wind speed; and wind vectors plotted every 10 days.

with low-passed values under 0.01 mm h^{-1}. Neither net longwave radiation nor sensible heat flux had clear annual signals. Reduced net shortwave heat flux in austral winter together with slightly increased latent heat flux in fall, winter, and spring led to oceanic heat loss at the sea surface from early April to late August. The occurrence of the maximum wind stress in the late austral winter was roughly coincident with the transition back from cooling of the ocean by the atmosphere to heating by the atmosphere.

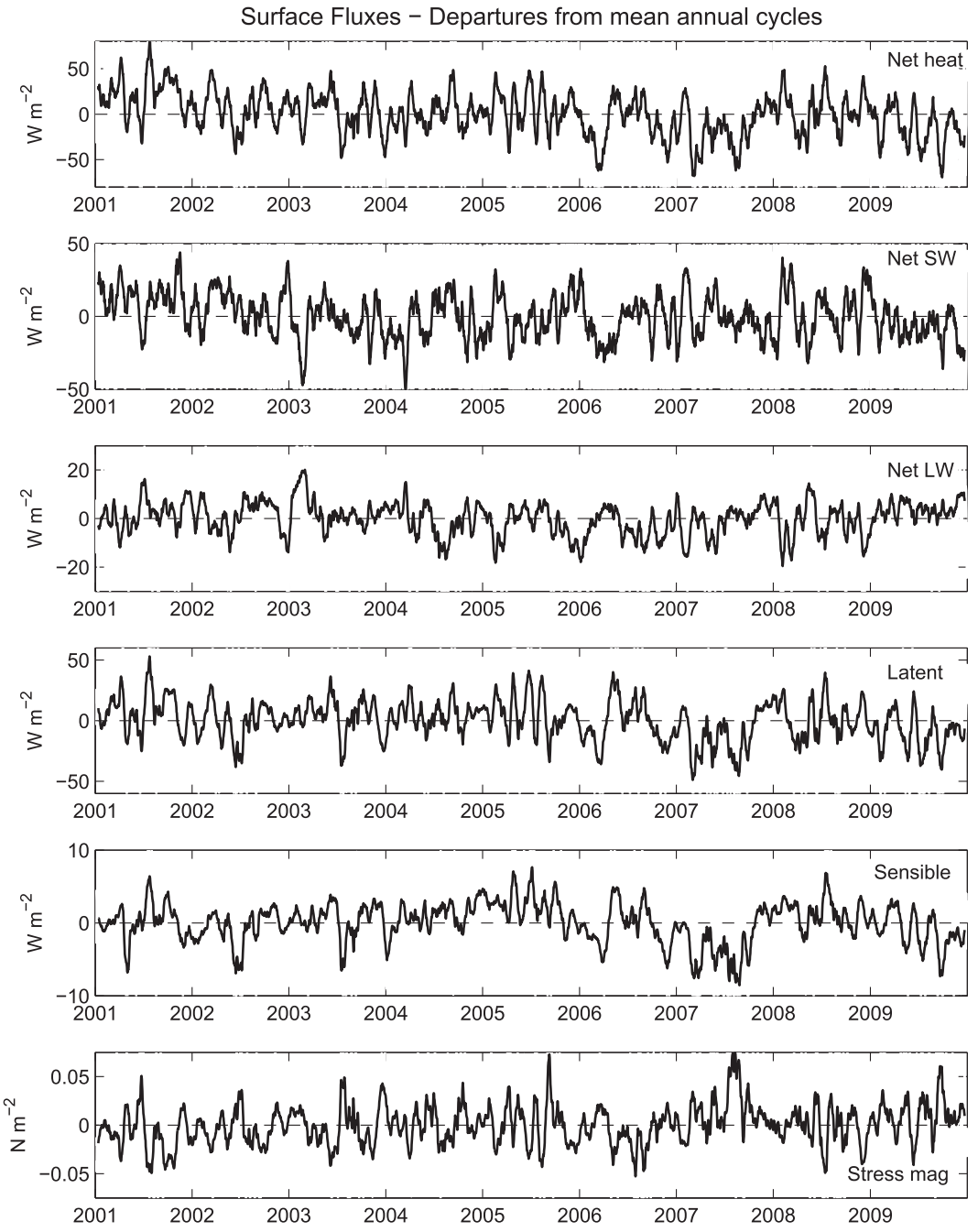

FIG. 7. The departures of the daily heat fluxes and wind stress from the annual mean cycles shown in Fig. 5. Shown are (top)–(bottom) net heat flux; net shortwave radiation; net longwave radiation; latent heat flux; sensible heat flux; and magnitude of the wind stress. All are daily time series with a 20-day running mean applied.

5. Interannual variability

Removing the annual mean cycle of daily averages in the surface meteorology and surface fluxes from each year of the daily time series yields time series of the departures from the mean annual cycle. The most prominent departures in the surface meteorology were cool events in air and sea surface temperatures in 2006 and again from early 2007 to early 2008 (Fig. 6). These were accompanied by a period of lower specific humidity and stronger trade winds. In the time series of the departures in the daily mean fluxes from the

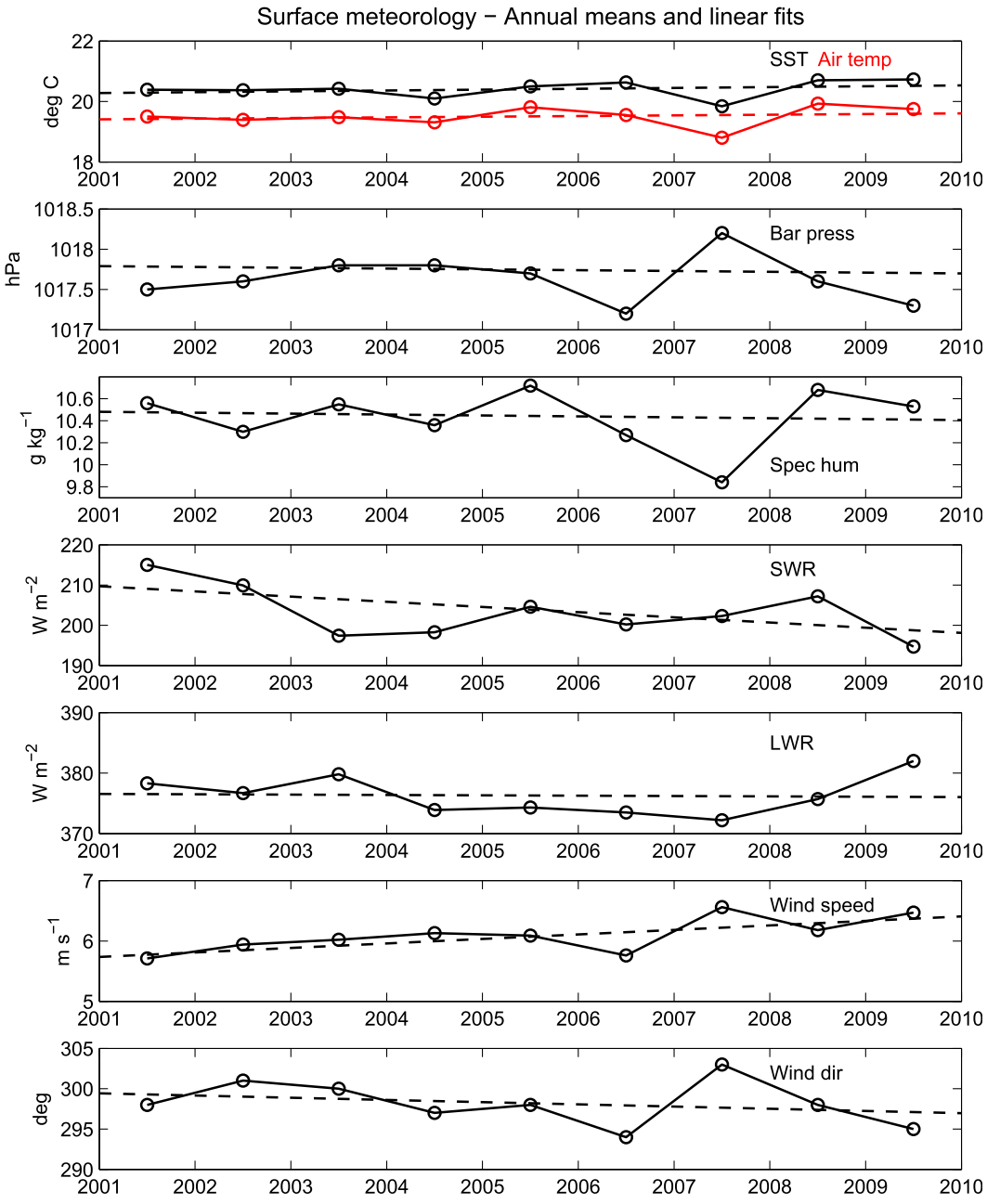

FIG. 8. Annual means of the surface meteorological variables with linear regression fits (dashed lines). Shown are (top)–(bottom) sea surface (black) and air (red) temperature; barometric pressure; specific humidity; incoming shortwave radiation; incoming longwave radiation; wind speed; and wind direction.

mean annual cycle (Fig. 7), distinct events were less apparent. Net heat fluxes were lower during the cold events and during the period of increased wind stress in mid-2007, with larger negative sensible and latent heat fluxes being the source of the negative net heat flux anomalies. There was not a suggestion from the net shortwave and net longwave anomalies of a significant change in cloud cover associated with these events.

6. Trends

To examine if trends were present with statistical significance linear regression analyses were carried out on the annual means. The annual means and fitted lines are shown in Fig. 8 (surface meteorology) and Fig. 9 (air–sea fluxes). Testing the hypotheses that the resulting slopes were significantly nonzero pointed to statistical significance in only the annually averaged wind speed and the

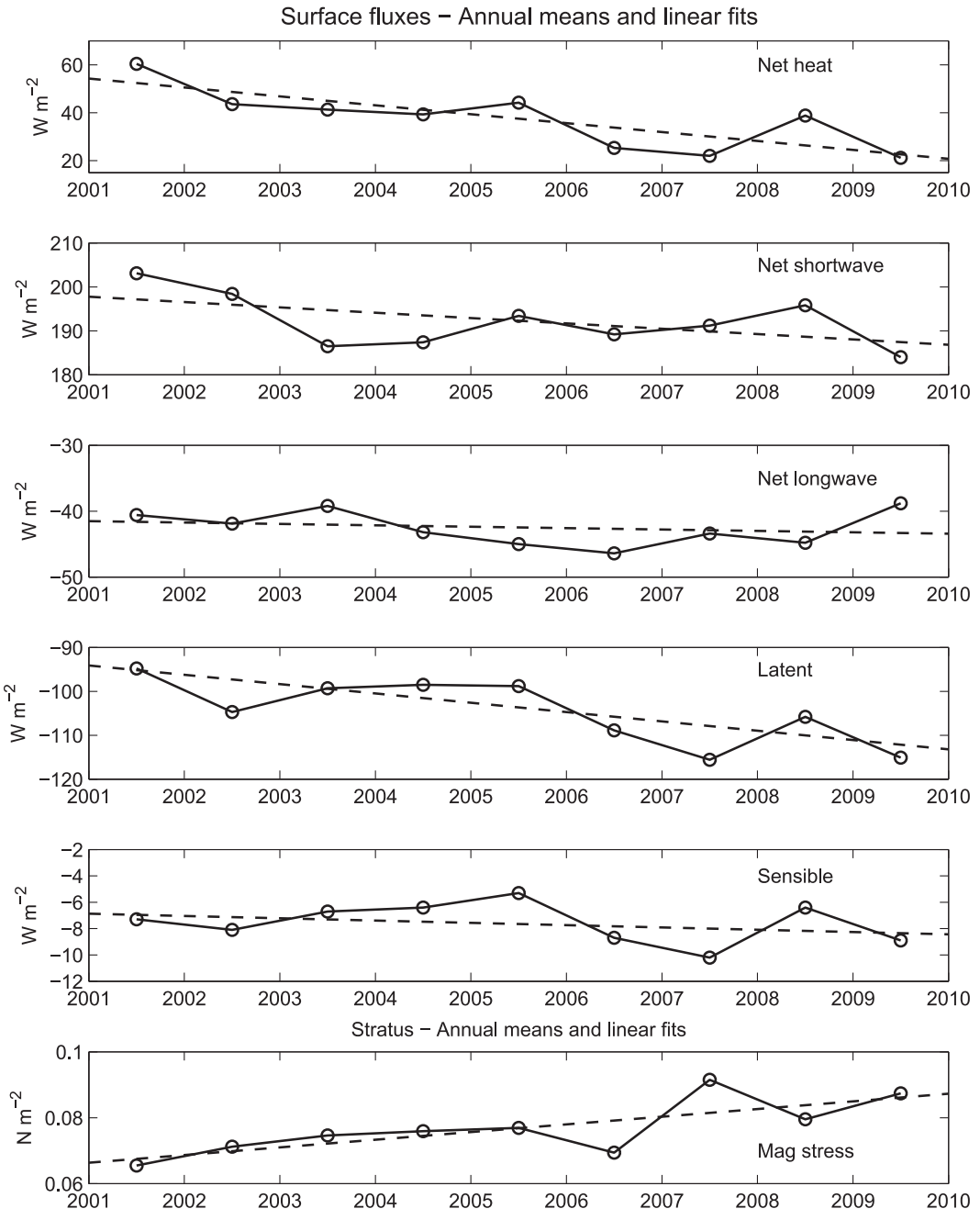

FIG. 9. Annual means of the air–sea flux variables with linear regression fits (dashed lines). Shown are (top)–(bottom) net heat flux; net shortwave radiation; net longwave radiation; latent heat flux; sensible heat flux; and the magnitude of the wind stress.

annually averaged east wind component, with the slope in wind speed close to $0.075\,\mathrm{m\,s^{-1}\,yr^{-1}}$ and in the east wind component close to $-0.121\,\mathrm{m\,s^{-1}\,yr^{-1}}$ (Table 5). Linear regression analyses of the annual mean values of the fluxes pointed to slopes that were statistically significantly different from zero for net heat flux, latent heat flux, the magnitude of the wind stress, and the east component of the wind stress (Table 6). Net heat flux decreased with time at a rate of $-3.73\,\mathrm{W\,m^{-2}\,yr^{-1}}$, with latent heat flux becoming more negative at $-2.12\,\mathrm{W\,m^{-2}\,yr^{-1}}$.

The increases in wind speed, wind stress, and latent heat flux over 9 yr were $0.8\,\mathrm{m\,s^{-1}}$, $0.022\,\mathrm{N\,m^{-2}}$, and $20\,\mathrm{W\,m^{-2}}$ or 13%, 29%, and 20% of the 9-yr means, respectively. The decrease in the annual mean net heat

TABLE 5. Linear regressions of the surface meteorological variables where the slope is significantly nonzero, wind speed, and the east component of wind. The 95% confidence interval (CI) for the slope are given. The term R^2 is the square of the correlation coefficient between the variable and time. The p value is for testing the null hypothesis that there is no trend with time (slope = 0); a low p value supports rejecting the null hypothesis.

	Slope ($m\,s^{-1}\,yr^{-1}$)	95% CI	R^2	p
Wind speed	0.075 ± 0.028	0.009 to 0.140	0.5096	0.0308
East wind	−0.121 ± 0.036	−0.207 to −0.036	0.6161	0.0122

flux was 39 $W\,m^{-2}$ or 104% of the mean. If these trends persist, the annual mean net air–sea heat flux will change sign by 2016, when the magnitude of the wind stress will have increased by close to 60%.

To examine whether the statistics of these trends across the nine years for a given season or for the annual mean were dominated by a high amplitude subset of the daily averages, the histograms of the daily averages for each year and season were examined. Overplotting the histograms and the annual means and medians pointed to a shift over the years in the distributions (Fig. 10). The 2009 histogram of the magnitude of the wind stress had a broader peak at slightly higher values and a small number of stronger events. The 2009 histogram of daily averaged net heat flux was shifted toward stronger heat losses, with a broader central peak. The 2009 histogram of daily averaged latent heat flux was also shifted toward larger negative values, with more higher heat loss values and fewer lower heat loss values. With the exception of the 2007 histograms, which reflected the interannual variability discussed in section 5, the temporal evolution of these year-by-year histograms of daily means showed a steady shift in means, medians, and overall distributions.

The nature of the long-term trends was examined further from the perspective of looking at the seasonal dependence in the trends. The data were subsetted into the four seasons: December–February (austral summer), March–May (austral fall), June–August (austral winter), and September–November (austral spring). Then the regression analyses were carried out season by season. The wind speed and wind stress magnitude trends were significant for fall and spring; the trends in east wind and east wind stress were significant for spring; and the trend for north wind stress was significant for spring (Tables 7 and 8). The trends in the net heat flux and the latent heat flux were significant in fall and spring (Table 8). No significantly nonzero slopes in the fits to surface meteorological and air–sea flux variables were found for summer or winter. The significant trends came from austral spring and fall, and the trends in austral spring were stronger than those in fall or the annual averages.

7. Discussion

The ORS STRATUS data show a trade wind regime characterized by directionally steady southeast trade winds. There is an annual cycle, most evident in moderate strengthening of the wind in late winter and in the seasonal cycle in solar insolation. In addition, there is interannual variability, most evident between 2006 and 2009. There are statistically significant trends in the wind velocity, wind stress, net heat flux, and latent heat flux. Looking at different seasons, it is the austral fall and spring that have the strongest trends.

The annual variability stems from two sources. One source is the large-scale surface wind circulation. The role of the South Pacific high pressure center in establishing the mean state has been noted by Rahn and Garreaud (2010a) and others. Garreaud (2011) discusses the annual migration and modulation of the southeastern Pacific anticyclone; during austral summer it is slightly weaker and more to the south, while during austral winter it is more intense and farther north. This can be seen in the sea level pressure fields from the National Centers for Environmental Prediction (NCEP)–U.S. Department of Energy (DOE) Reanalysis-2 (Kanamitsu et al. 2002), which show in a typical year a shift toward the east in austral winter and spring of the center of the South Pacific high pressure cell, which both raises the pressure at the ORS STRATUS and creates a stronger pressure gradient spanning that location. The second source of annual variability in the surface meteorology and air–sea fluxes is the astronomical annual cycle in incoming shortwave radiation. The solar variability is a major contributor to the observed annual cycle in neat heat flux; the insolation decreases enough in austral winter

TABLE 6. Linear regressions of fluxes where the slope is significantly nonzero.

	Slope	95% CI	R^2	p
Net heat	−3.73 ± 1.03 $W\,m^{-2}\,yr^{-1}$	−6.17 to −1.29	0.6507	0.0086
Latent heat	−2.12 ± 0.65 $W\,m^{-2}\,yr^{-1}$	−3.66 to −0.590	0.6053	0.0136
Wind stress magnitude	0.002 33 ± 0.000 74 $N\,m^{-2}\,yr^{-1}$	0.000 582 to 0.004 08	0.5871	0.0161
East wind stress	−0.002 60 ± 0.000 62 $N\,m^{-2}\,yr^{-1}$	−0.004 18 to −0.001 02	0.6831	0.0060

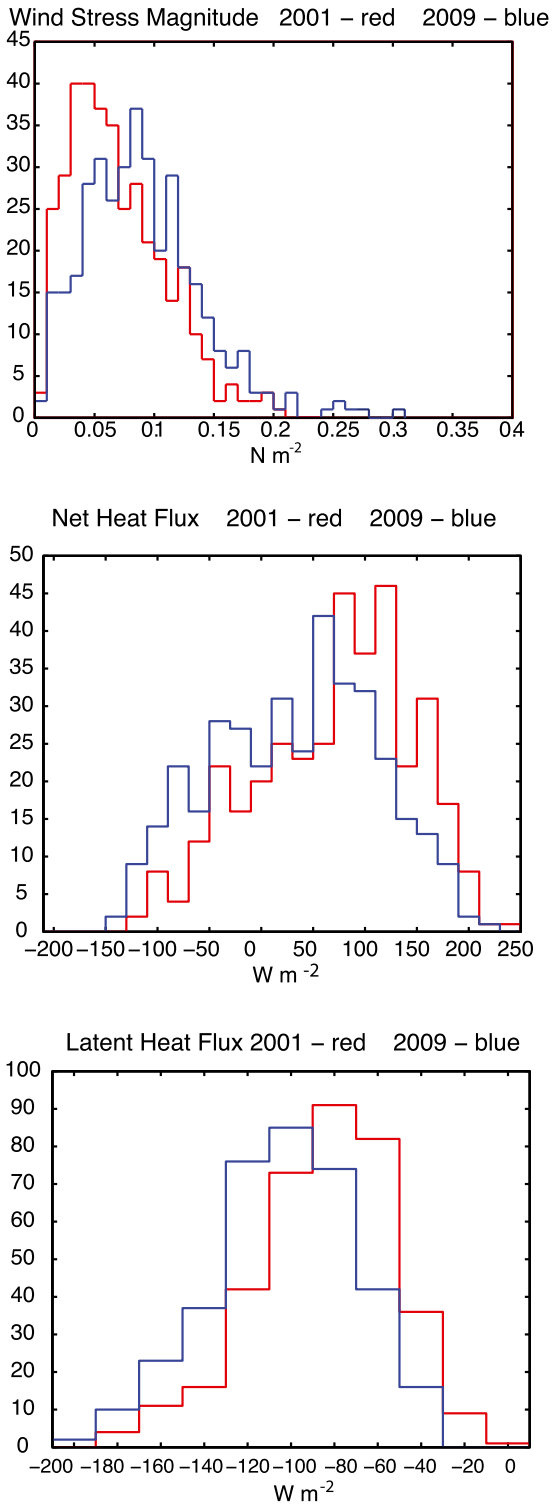

FIG. 10. Overplots to contrast the histograms in 2001 (red) and in 2009 (blue) of daily averages of the magnitude of (top) the wind stress, (middle) the net heat flux, and (bottom) the latent heat flux.

so that the mean annual cycle shows ocean heat loss from early April to mid-August.

The source of the interannual variability is not as clear. In Fig. 11, additional smoothing beyond that used in Fig. 6 has been applied to the time series of daily departures from the annual means of wind stress and net heat flux, and these have been plotted against SST and surface salinity. The increased trade winds in 2007 and the more negative net heat fluxes between 2006 and 2009 show evidence of covariance with SST and surface salinity.

The coastal waters of the eastern South Pacific experience variability associated with El Niño–Southern Oscillation (ENSO), and two ENSO indices are included in Fig. 11. The Niño-1+2 region lies between the equator and 10°S and between 80° and 90°W, north of the ORS STRATUS. Another measure of ENSO variability is the multivariate ENSO index (MEI) developed by Wolter and Timlin (1998). Figure 11 shows the alignment of the cool, fresh events of 2006 and 2007/08 with SST variability in the Niño-1+2 index and to a lesser extent in the MEI. The negative net heat flux anomalies as large as $-40\,\mathrm{W\,m^{-2}}$ in 2006 and 2007/08 are seen in Fig. 10, coincident with cool anomalies in the Niño-1+2 and MEI temperatures.

The cooler, fresher conditions at the buoy for 1–2 months in early 2007 lag a weak La Niña event, whereas the cooler, fresher conditions over the latter half of 2007 are aligned with a moderate La Niña event. The increased wind stress in the middle of 2007 lasted 2–3 months, a period shorter than the La Niña occurring at that time. It is probable that interannual variability at the ORS STRATUS has other sources in addition to ENSO. Investigations of rainfall in central and north-central Chile (Rutllant and Fuenzalida 1991; Julia et al. 2012) point to the influence of the region around the Antarctic Peninsula in addition to the Southern Oscillation and the Madden–Julian oscillation. Other work (Mo and White 1985) has pointed to large-scale patterns of seasonal variability in the Southern Hemisphere that span from low to high latitudes. Because there is little rain at and near the ORS STRATUS, the freshening of the surface water in 2006–09 also suggests that ocean dynamics influence surface properties and may, through SST, influence local meteorology and air–sea fluxes. Holte et al. (2014) have concluded that advection of cooler, fresher water makes the same order of magnitude contribution at the ORS STRATUS to upper-ocean heat and freshwater budgets as the surface fluxes do. In the face of this complexity, it was difficult to further investigate the interannual variability at the ORS STRATUS. It is clear, though, in 2006–08 that a contribution to the annual mean statistics is seen from

TABLE 7. Linear regressions of surface meteorological variables by season where the slope is significantly nonzero.

	Slope ($m\,s^{-1}\,yr^{-1}$)	95% CI	R^2	p
Wind speed: fall	0.074 ± 0.026	0.013 to 0.134	0.4966	0.0229
Wind speed: spring	0.129 ± 0.030	0.059 to 0.200	0.7304	0.0033
East wind: spring	−0.149 ± 0.031	−0.222 to −0.075	0.7656	0.0020

the interannual variability and that those annual means fall further off the linear fit lines in Figs. 9 and 10.

The trends associated with these linear fits are of interest. There are a number of remarks about regional trends in the literature. Ramage (1987) cautioned about interpreting trends in historical data, such as in the Comprehensive Ocean–Atmosphere Data Set (COADS; Slutz et al. 1985), which spans from 1854 to the present. However, Jahncke et al. (2004) concluded that off Peru, near 13°S, 79°W, the COADS data in the 1925–2000 period showed increasing annual mean meridional wind stress, with a slope of $35.9 \times 10^{-5}\,N\,m^{-2}\,yr^{-1}$. Bakun's (1990) discussion of intensifying coastal upwelling based on analysis of ship data from 1946 to 1988 in four different coastal upwelling regions pointed to long-term, statistically significant, positive trends in alongshore wind stress off Peru. However, his plots of October–March and April–September wind stress off Peru also showed strong decadal variability. Independent of wind data, Vargas et al.'s (2007) analysis of sediment cores suggest that upwelling has increased since 1878 in association with intensification of the winds driving the upwelling.

Falvey and Garreaud (2009) discussed temperature trends along the Chilean coast and reported cooling of $-0.07°C\,decade^{-1}$; they suggested this was occurring in association with an intensification of the southeastern Pacific anticyclone. Their analysis of reanalysis and model data showed increasing sea level pressures in the South Pacific high located west of Chile. Garreaud and Falvey (2009) discuss change in the wind regime off Chile under future climate scenarios. In global climate models, they find an increase of $0.4\,m\,s^{-1}$ over 100 yr at the STRATUS site. Using a regional climate model, they suggest an increase and found the broad region of trade winds from the southeast offshore of northern Chile and the region of southerlies along the central Chile coast to be increasing.

In contrast, Vecchi et al. (2006) suggest that the Walker circulation will weaken and that the trade winds off Peru will weaken in a warming future climate. Vecchi and Soden (2007) also indicate that the tropical atmospheric circulation weakens as climate warms in all Intergovernmental Panel on Climate Change (IPCC) AR4 models. However, many investigations of models provide support for strengthening Pacific trade winds. Merrifield et al. (2009) noted strong sea level rise in western tropical Pacific, and Merrifield and Maltrud (2011) found one cause of that sea level rise to be the increased strength of Pacific trade winds on multidecadal time scales. They looked at ECMWF winds over the period of 1993–2010 and used these winds to force an ocean model. Timmermann and McGregor (2010), when looking at sea level under two Intergovernmental Panel on Climate Change scenarios A1B and B1 found increased southeasterly winds in the South Pacific to be a robust result in model simulations.

Because of the societal importance of the fisheries in the region of upwelling along the coast of Peru and Chile, there have been a number of studies of trends and variability in SST, winds, and productivity. Demarcq (2009), using SeaWinds scatterometer winds from 2000 to 2007, reported an increase in the equatorward winds off northern Chile and Peru in the upwelling zones of $0.2–0.3\,m\,s^{-1}\,decade^{-1}$, in conjunction with little change in SST off Peru and a slight cooling in SST off northern Chile ($-0.15°C\,decade^{-1}$) and increases in productivity

TABLE 8. Linear regressions of the air–sea flux variables by season where the slope is significantly nonzero.

	Slope	95% CI	R^2	p
Wind stress magnitude: fall	$0.002\,10 \pm 0.000\,64\,W\,m^{-2}\,yr^{-1}$	0.006 13 to 0.003 58	0.5703	0.0116
Wind stress magnitude: spring	$0.004\,18 \pm 0.000\,89\,W\,m^{-2}\,yr^{-1}$	0.002 07 to 0.006 29	0.7584	0.0022
Tau east: fall	$-0.002\,36 \pm 0.000\,67\,W\,m^{-2}\,yr^{-1}$	−0.003 90 to −0.000 82	0.6097	0.0077
Tau east: spring	$-0.004\,06 \pm 0.000\,81\,W\,m^{-2}\,yr^{-1}$	−0.005 96 to −0.002 15	0.7837	0.0015
Tau north: spring	$0.001\,67 \pm 0.000\,66\,W\,m^{-2}\,yr^{-1}$	0.000 12 to 0.003 22	0.4813	0.0382
Net heat: fall	$-4.35 \pm 1.34\,W\,m^{-2}\,yr^{-1}$	−7.43 to −1.28	0.5707	0.0115
Net heat: spring	$-5.17 \pm 1.05\,W\,m^{-2}\,yr^{-1}$	−7.64 to −2.70	0.773	0.0017
Latent heat: fall	$-2.38 \pm 0.96\,W\,m^{-2}\,yr^{-1}$	−4.59 to −0.17	0.4345	0.0382
Latent heat: spring	$-2.96 \pm 0.77\,W\,m^{-2}\,yr^{-1}$	−4.78 to −1.14	0.6796	0.0063

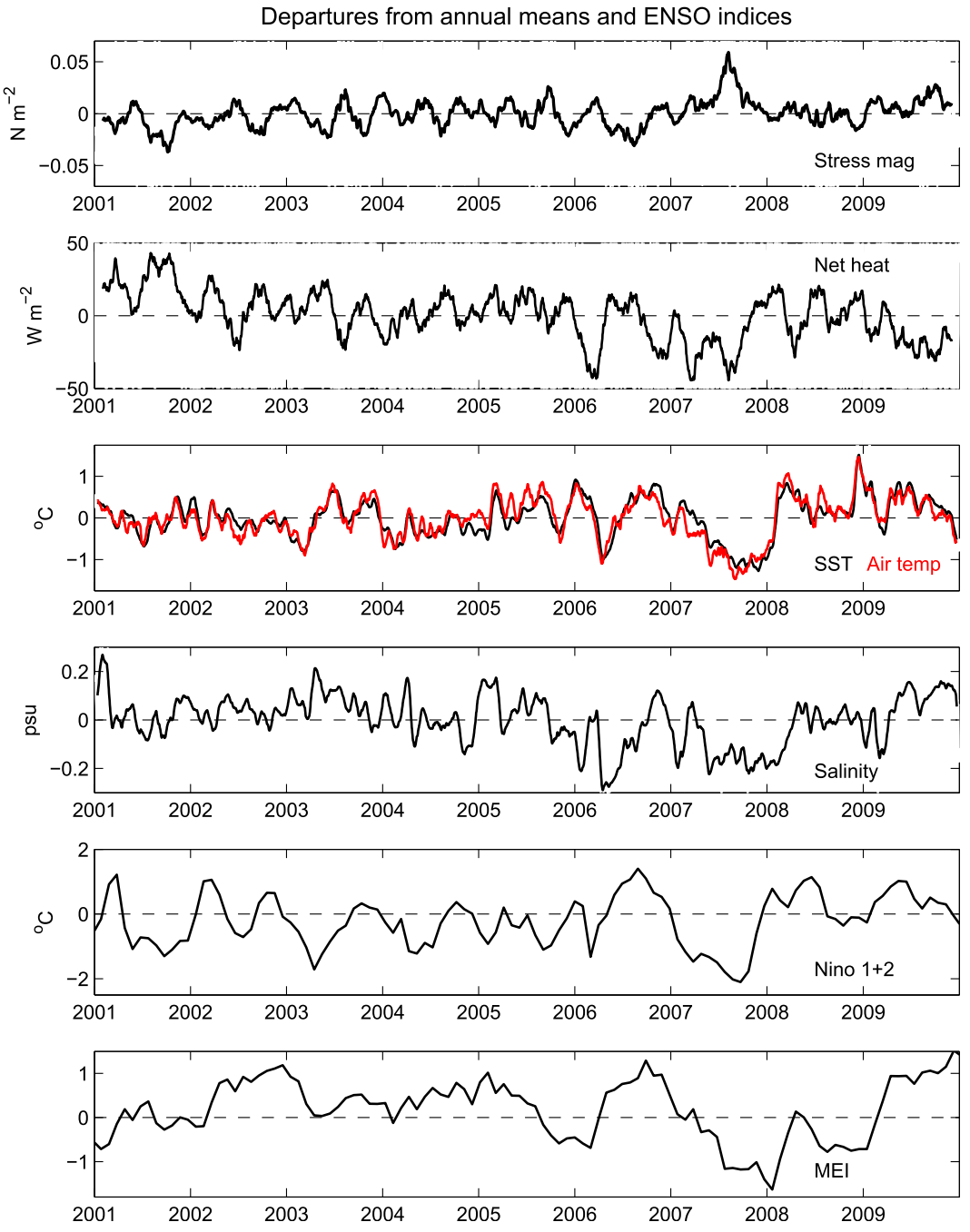

FIG. 11. Time series of the departures of daily values from the mean annual cycle for (top)–(bottom) wind stress magnitude; daily net heat flux; air temperature (red) and SST (black) together; sea surface salinity; the monthly Niño-1+2 temperature anomaly [from NCEP Climate Prediction Center (CPC): http://www.cpc.ncep.noaa.gov/data/indices/sstoi.indices]; and the monthly MEI after Wolter and Timlin (1998) (obtained at http://www.esrl.noaa.gov/psd/enso/mei/table.html). A 60-day running mean has been applied to the stress and net heat flux daily time series and a 20-day running mean has been applied to the SST, air temperature, and salinity.

off both Peru and northern Chile. Gutiérrez et al. (2011) used a proxy for SST derived from sediment samples off Peru and point to a combination of increased productivity and cooling of SST; they suggest that the increasing winds seen in the 40-yr ECMWF Re-Analysis (ERA-40) are driving increased upwelling.

Table 9 summarizes values of trends in surface wind speed and wind stress in the eastern South Pacific from

TABLE 9. Summary of wind speed and wind stress trends. G. W. Moore (2014, personal communication) are values provided by G. W. Moore's analyses of ERA-Interim fields. Values from the literature are extracted from figures and tables.

Source	Time period	Wind speed trend ($m\,s^{-1}\,decade^{-1}$)	Wind stress trend ($N\,m^{-2}\,decade^{-1}$)	Note
Jahncke et al. (2004)	1925–2000	—	3.59×10^{-3}	Off Peru
Bakun (1990)	1946–88	—	$3.5–3.8 \times 10^{-3}$	—
Garreaud and Falvey (2009)	2071–2100 and 1961–2000	0.04	—	—
Merrifield and Maltrud (2011)	1993–2010	—	2×10^{-2}	—
Timmermann and McGregor (2010)	2001–2100	—	0.05×10^{-4}	—
G. W. Moore (2014, personal communication)	1986–99	0.3	—	—
G. W. Moore (2014, personal communication)	2000–13	0.5	—	—
Kosaka (2014)	2000–13	0.3	—	—
England et al. (2014)	1992–2011	—	1×10^{-2}	—
This paper	2000–09	0.75	2.3×10^{-2}	Annual: wind vector
This paper	2000–09	−1.21	-2.6×10^{-2}	Annual: zonal component
This paper	2000–09	1.29	4.2×10^{-2}	Spring: wind vector
This paper	2000–09	−1.49	-4.1×10^{-2}	Spring: zonal component

the literature and from G. W. Moore (2014, personal communication). There is general agreement that the wind speed and wind stress are increasing. The ORS STRATUS data from 2000 to 2009 suggest that, if the present trends for wind stress and net heat flux persist, by 2016 the sign of the annual mean net air–sea would change and, on an annual mean, the ocean would lose heat. This would lead to net cooling. The increased latent heat loss would at the same time by evaporation further increase the density of the surface layer of the ocean. Thus, there is nonstationarity in the surface forcing of the ocean by the atmosphere off northern Chile, and investigations of upper-ocean heat budgets and ocean dynamics there should acknowledge this.

8. Conclusions

A well-instrumented surface mooring has been deployed near 20°S, 85°W since October 2000. The surface meteorological and air–sea flux data have been carefully quality controlled, and the uncertainties of the data are well known. These data have been withheld from near-real-time assimilation into weather and climate models. As such, they provide a good resource for evaluating models.

In this paper, nine full calendar years of data were used to construct a mean annual cycle and characterize annual means. Removing the mean annual cycle makes more evident the observed interannual variability in 2007–08. Working with the annual means, statistically significant trends were found in wind speed, the east component of the wind, the magnitude of the wind stress, the east component of the wind stress, the net heat flux, and the latent heat flux. The change over the years is not due to a small number of extreme valued events; the histograms of daily values showed change across all the population. When the data were further broken down by season as well as by year, the changes in

TABLE A1. Locations and dates of the mooring deployments from October 2000 to July 2010. Deployment is the date and time of anchor drop. Recovery is the date and time when the mooring is released from the anchor, except for STRATUS 10, when the date the surface buoy began to drift away for the site after a failure in the mooring is given. The surface buoy of these moorings, which have a length about 1.25 times the water depth, moves around during the deployment in response to the ocean currents within a watch circle of roughly 5-km radius centered on the anchor site.

	Deployment	Recovery	Latitude	Longitude
STRATUS 1	2043 UTC 7 Oct 2000	1239 UTC 17 Oct 2001	20°09.42′S	85°09.07′W
STRATUS 2	1946 UTC 19 Oct 2001	1259 UTC 22 Oct 2002	20°08.60′S	85°08.44′W
STRATUS 3	0016 UTC 25 Oct 2002	1232 UTC 17 Nov 2003	20°10.48′S	85°06.73′W
STRATUS 4	2031 UTC 19 Nov 2003	1047 UTC 12 Dec 2004	19°45.95′S	85°30.41′W
STRATUS 5	1825 UTC 14 Dec 2004	1045 UTC 12 Oct 2005	19°44.74′S	85°31.36′W
STRATUS 6	1751 UTC 14 Oct 2005	1245 UTC 18 Oct 2006	20°02.67′S	85°11.31′W
STRATUS 7	1751 UTC 16 Oct 2006	1057 UTC 29 Oct 2007	19°45.28′S	85°31.93′W
STRATUS 8	1827 UTC 27 Oct 2007	1045 UTC 27 Oct 2008	19°37.36′S	85°22.73′W
STRATUS 9	1846 UTC 25 Oct 2008	1137 UTC 20 Jan 2010	19°42.65′S	85°35.25′W
STRATUS 10	1823 UTC 17 Jan 2010	7 Jul 2010	19°36.81′S	85°23.12′W

wind speed, wind stress, latent heat flux, and net heat flux were strongest in spring and fall.

Continuing observations at the ORS STRATUS are needed to show whether the 2000–09 trends will persist or if they are representative of just a phase of a decadal or multidecadal mode of variability. Sustained increase in the southeast trade winds in the South Pacific and the associated increase in upwelling along the west coast of South America should have consequences on the ecosystem there. Given the modest net heat gain and strong evaporation there, the trend in net heat flux, if continued, will shift by about 2016 in the region from one of net annual heat gain by the ocean from atmosphere to one of net annual heat loss. At the same time, the increased evaporation will lead to denser surface water and the increased wind stress may increase wind-driven shear across the base of the surface mixed layer. These changes could both lead to change in the structure of the upper ocean in the region.

Among the challenges faced in developing an improved understanding of the eastern South Pacific and in improving model performance, there is thus the finding that there are significant trends in the surface meteorology and in the air–sea exchanges of heat, freshwater, and momentum. The ORS STRATUS time series provide documented in situ records of surface meteorology and air–sea fluxes that have not, when collected, been used in operational models. As such, they provide a good means not only to investigate and understand the variability of the region but also to examine model performance in the region. These time series are available online (at http://uop.whoi.edu/ReferenceDataSets/index.html).

Acknowledgments. Dr. Chris Fairall of NOAA is thanked for providing the shipboard meteorological and air–sea flux instrumentation on the research vessels on many of the cruises; these are essential to establishing and maintaining the accuracies of the moored instrumentation. This work is supported by the NOAA Climate Observation Division (NA09OAR4320129). The technical staff of the Upper Ocean Processes Group at the Woods Hole Oceanographic Institution and the crews of the NOAA and UNOLS vessels and crews have been essential to the successful long-term maintenance of Ocean Reference Stations. NCEP–DOE Reanalysis-2 data are provided by the NOAA/OAR/ESRL PSD, Boulder, Colorado, from their website (at http://www.esrl.noaa.gov/psd/). Discussions with G. W. Moore provided insight and motivation and are gratefully acknowledged. The input from two anonymous reviewers, which lead to improvements in the manuscript, is gratefully acknowledged.

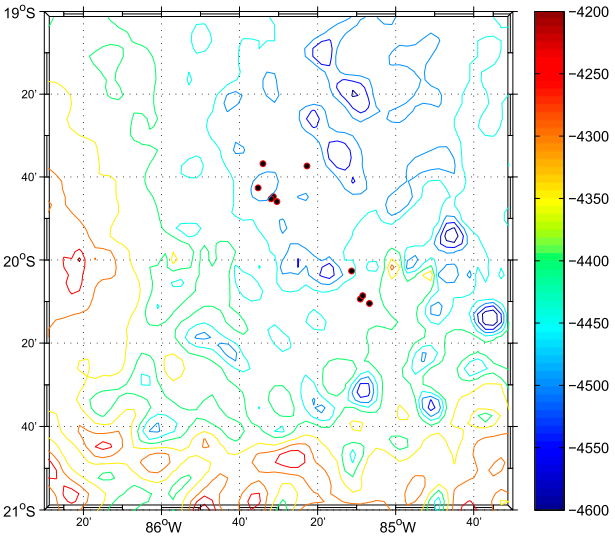

FIG. A1. Locations of the first 10 deployments of the STRATUS moorings plotted with red dots on top of the bathymetry (m).

APPENDIX

Mooring Locations

Table A1 provides a list of the locations of the anchor positions for each of the 10 deployments of the ORS STRATUS. Figure A1 shows the locations on top of the local bathymetry.

REFERENCES

Bakun, A., 1990: Global climate change and intensification of coastal ocean upwelling. *Science,* **247,** 198–201, doi:10.1126/science.247.4939.198.

Bigorre, S. P., R. A. Weller, J. B. Edson, and J. D. Ware, 2013: A surface mooring for air–sea interaction research in the Gulf Stream. Part II: Analysis of the observations and their accuracies. *J. Atmos. Oceanic Technol.,* **30,** 450–469, doi:10.1175/JTECH-D-12-00078.1.

Colbo, K., and R. Weller, 2007: The variability and heat budget of the upper ocean under the Chile-Peru stratus. *J. Mar. Res.,* **65,** 607–637, doi:10.1357/002224007783649510.

——, and ——, 2009: Accuracy of the IMET sensor package in the subtropics. *J. Atmos. Oceanic Technol.,* **26,** 1867–1890, doi:10.1175/2009JTECHO667.1.

Cronin, M. F., N. A. Bond, C. W. Fairall, and R. A. Weller, 2006: Surface cloud forcing in the east Pacific stratus deck/cold tongue/ITCZ complex. *J. Climate,* **19,** 392–409, doi:10.1175/JCLI3620.1.

Demarcq, H., 2009: Trends in primary production, sea surface temperature, and wind in upwelling systems (1998-2007). *Prog. Oceanogr.,* **83,** 376–385, doi:10.1016/j.pocean.2009.07.022.

De Szoeke, S. P., C. W. Fairall, D. E. Wolfe, L. Bariteau, and P. Zuidema, 2010: Surface flux observations on the southeaster tropical Pacific Ocean and attribution of SST errors in coupled ocean–atmosphere models. *J. Climate,* **23,** 4152–4174, doi:10.1175/2010JCLI3411.1.

England, M. H., and Coauthors, 2014: Recent intensifications of wind-driven circulation in the Pacific and the ongoing

warming hiatus. *Nat. Climate Change,* **4,** 222–227, doi:10.1038/nclimate2106.

Fairall, C. W., E. F. Bradley, D. P. Rogers, J. B. Edson, and G. S. Young, 1996: Bulk parametrization of air-sea fluxes for Tropical Ocean Global Atmosphere Coupled Ocean-Atmosphere Response Experiment. *J. Geophys. Res.,* **101,** 3747–3764, doi:10.1029/95JC03205.

Falvey, M., and R. D. Garreaud, 2009: Regional cooling in a warming world: Recent temperature trends in the southeast Pacific and along the west coast of subtropical South America (1979–2006). *J. Geophys. Res.,* **114,** D04102, doi:10.1029/2008JD010519.

Garreaud, R. D., 2011: The climate of northern Chile: Mean state, variability and trends. *Rev. Mex. Astron. Astrofis.,* **41,** 5–11.

——, and M. Falvey, 2009: The coastal winds off western subtropical South America in future climate scenarios. *Int. J. Climatol.,* **29,** 543–554, doi:10.1002/joc.1716.

Gutiérrez, D., and Coauthors, 2011: Coastal cooling and increased productivity in the main upwelling zone off Peru since the mid-twentieth century. *Geophys. Res. Lett.,* **38,** L07603, doi:10.1029/2010GL046324.

Holte, J., F. Straneo, J. T. Farrar, and R. A. Weller, 2014: Heat and salinity budgets at the Stratus mooring in the southeast Pacific. *J. Geophys. Res. Oceans,* **119,** 8162–8176, doi:10.1002/2014JC010256.

Hosom, D. S., R. A. Weller, R. E. Payne, and K. E. Prada, 1995: The IMET (improved meteorology) ship and buoy systems. *J. Atmos. Oceanic Technol.,* **12,** 527–540, doi:10.1175/1520-0426(1995)012<0527:TIMSAB>2.0.CO;2.

Iqbal, M., 1988: *Physical Climatology for Solar and Wind Energy.* World Scientific, 1086 pp.

Jahncke, J., D. M. Checkley Jr., and G. L. Hunt Jr., 2004: Trends in carbon flux to seabirds in the Peruvian upwelling system: Effects of wind and fisheries on population regulation. *Fish. Oceanogr.,* **13,** 208–223, doi:10.1111/j.1365-2419.2004.00283.x.

Julia, C., D. A. Rahn, and J. A. Rutllant, 2012: Assessing the influence of the MJO on strong precipitation events in subtropical, semi-arid north-central Chile (30°S). *J. Climate,* **25,** 7003–7013, doi:10.1175/JCLI-D-11-00679.1.

Kanamitsu, M., W. Ebisuzaki, J. Woollen, S.-K. Yang, J. J. Hnilo, M. Fiorino, and G. L. Potter, 2002: NCEP–DOE AMIP-II Reanalysis (R-2). *Bull. Amer. Meteor. Soc.,* **83,** 1631–1643, doi:10.1175/BAMS-83-11-1631.

Kosaka, Y., 2014: Increasing wind sinks heat. *Nat. Climate Change,* **4,** 172–173, doi:10.1038/nclimate2138.

Large, W. G., and G. Danabasoglu, 2006: Attribution and impacts of upper-ocean biases in CCSM3. *J. Climate,* **14,** 2325–2346, doi:10.1175/JCLI3740.1.

Ma, C.-C., C. R. Mechoso, A. W. Robertson, and A. Arakawa, 1996: Peruvian stratus clouds and the tropical Pacific circulation—A coupled ocean–atmosphere GCM study. *J. Climate,* **9,** 1635–1645, doi:10.1175/1520-0442(1996)009<1635:PSCATT>2.0.CO;2.

Manganello, J. V., and B. Huang, 2009: Sensitivity of the NCEP Climate Forecast System to changes in the SST bias. Part I: Tropical Pacific mean state. COLA Tech Rep. 29, 20 pp.

Mechoso, C. R., and Coauthors, 2013: Ocean–cloud–atmosphere–land interactions in the southeastern Pacific: The VOCALS program. *Bull. Amer. Meteor. Soc.,* **95,** 357–375, doi:10.1175/BAMS-D-11-00246.1

Merrifield, M. A., and M. E. Maltrud, 2011: Regional sea level trends due to a Pacific trade wind intensification. *Geophys. Res. Lett.,* **38,** L21605, doi:10.1029/2011GL049576.

——, S. T. Merrifield, and G. T. Mitchum, 2009: An anomalous recent acceleration of global sea level rise. *J. Climate,* **22,** 5772–5781, doi:10.1175/2009JCLI2985.1.

Mo, K. C., and G. H. White, 1985: Teleconnections in the Southern Hemisphere. *Mon. Wea. Rev.,* **113,** 22–37, doi:10.1175/1520-0493(1985)113<0022:TITSH>2.0.CO;2.

Narayan, N., A. Paul, S. Mulitza, and M. Schulz, 2010: Trends in coastal upwelling intensity in the late 20th century. *Ocean Sci.,* **6,** 815–823, doi:10.5194/os-6-815-2010.

Rahn, D. A., and R. Garreaud, 2010a: Marine boundary layer over the subtropical southeast Pacific during VOCALS_REx—Part 1: Mean structure and diurnal cycle. *Atmos. Chem. Phys.,* **10,** 4491–4506, doi:10.5194/acp-10-4491-2010.

——, and ——, 2010b: Marine boundary layer over the subtropical southeast Pacific during VOCALS-REx—Part 2: Synoptic variability. *Atmos. Chem. Phys.,* **10,** 4507–4519, doi:10.5194/acp-10-4507-2010.

Ramage, C. S., 1987: Secular change in reported surface wind speeds over the ocean. *J. Climate Appl. Meteor.,* **26,** 525–528, doi:10.1175/1520-0450(1987)026<0525:SCIRSW>2.0.CO;2.

Rutllant, J., and R. Fuenzalida, 1991: Synoptic aspects of the central Chile rainfall variability associated with Southern Oscillation. *Int. J. Climatol.,* **11,** 63–76, doi:10.1002/joc.3370110105.

Slutz, R. J., S. J. Lubker, J. D. Hiscox, S. D. Woodruff, R. L. Jenne, P. M. Steurer, and J. D. Elms, 1985: Comprehensive Ocean-Atmosphere Data Set; release 1. NOAA Environmental Research Laboratories Climate Research Program, 268 pp.

Timmermann, A., and S. McGregor, 2010: Wind effects on past and future regional sea level trends in the southern Indo-Pacific. *J. Climate,* **23,** 4429–4437, doi:10.1175/2010JCLI3519.1.

Toniazzo, T., S. J. Abel, R. Wood, C. R. Mechoso, G. Allen, and L. C. Shaffrey, 2011: Large-scale and synoptic meteorology in the south-east Pacific during the observations campaign VOCALS-REx in austral spring 2008. *Atmos. Chem. Phys.,* **11,** 4977–5009, doi:10.5194/acp-11-4977-2011.

Vargas, G., S. Pantoja, J. A. Rutllant, C. B. Lange, and L. Ortlieb, 2007: Enhancement of coastal upwelling and interdecadal ENSO-like variability in the Peru-Chile current since late 19th century. *Geophys. Res. Lett.,* **34,** L13607, doi:10.1029/2006GL028812.

Vecchi, G. A., and B. J. Soden, 2007: Global warming and the weakening of the tropical circulation. *J. Climate,* **20,** 4316–4340, doi:10.1175/JCLI4258.1.

——, ——, A. T. Wittenberg, I. M. Held, A. Leetmann, and M. J. Harrison, 2006: Weakening of tropical Pacific atmospheric circulation due to anthropogenic forcing. *Nature,* **441,** 73–76, doi:10.1038/nature04744.

Weller, R. A., F. Bradley, and R. Lukas, 2004: The interface or air–sea flux component of the TOGA Coupled Ocean–Atmosphere Response Experiment and it impact on subsequent air–sea interaction studies. *J. Atmos. Oceanic Technol.,* **21,** 223–257, doi:10.1175/1520-0426(2004)021<0223:TIOAFC>2.0.CO;2.

——, S. P. Bigorre, J. Lord, and J. D. Ware, 2012: A surface mooring for air–sea interaction research in the Gulf Stream. Part I: Mooring design and instrumentation. *J. Atmos. Oceanic Technol.,* **29,** 1363–1376, doi:10.1175/JTECH-D-12-00060.1.

Wolter, K., and M. S. Timlin, 1998: Measuring the strength of ENSO events: How does 1997/98 rank? *Weather,* **53,** 315–324, doi:10.1002/j.1477-8696.1998.tb06408.x.

Zheng, Y., T. Shinoda, J.-L. Lin, and G. N. Kiladis, 2011: Sea surface temperature biases under the stratus cloud deck in the southeast Pacific Ocean in 19 IPCC AR4 coupled general circulation models. *J. Climate,* **24,** 4139–4164, doi:10.1175/2011JCLI4172.1.